Proteome-wide cross-linking mass spectrometry to identify specific virus capsid-host interactions between tick-borne encephalitis virus and neuroblastoma cells

Sarah V. Barrass[1,2], Lauri I. A. Pulkkinen[1,2], Olli Vapalahti[3,4,5], Suvi H. Kuivanen[3] ,Maria Anastasina[1,2*], Lotta Happonen[6*], Sarah J. Butcher[1,2*]

[1] Faculty of Biological and Environmental Sciences, Molecular and Integrative Bioscience Research Programme, University of Helsinki, Helsinki, Finland

[2] Helsinki Institute of Life Sciences-Institute of Biotechnology, University of Helsinki, Helsinki, Finland

[3] Department of Virology, University of Helsinki, Helsinki, Finland

[4] Department of Veterinary Biosciences, Faculty of Veterinary Medicine, University of Helsinki, Helsinki, Finland

[5] Division of Clinical Microbiology, University of Helsinki and Helsinki University Hospital, Helsinki, Finland

[6] Lund University, Faculty of Medicine, Department of Clinical Sciences Lund, Infection Medicine, Lund, Sweden

* Corresponding authors

Emails: sarah.butcher@helsinki.fi (SB), lotta.happonen@med.lu.se (LH), maria.anastasina@helsinki.fi (MA)

Abstract

Virus-host protein-protein interactions are central to viral infection, but are challenging to identify and characterise, especially in complex systems involving intact viruses and cells. In this work, we demonstrate a proteome-wide approach to identify virus-host interactions using chemical cross-linking coupled with mass spectrometry. We adsorbed tick-borne encephalitis virus onto metabolically-stalled neuroblastoma cells, covalently cross-linked interacting virus-host proteins, and performed limited proteolysis to release primarily the surface-exposed proteins for identification by mass spectrometry. Using the intraviral protein cross-links as an internal control to assess cross-link confidence levels, we identified 22 high confidence unique intraviral cross-links and 59 high confidence unique virus-host protein-protein interactions. The identified host proteins were shown to interact with eight distinct sites on the outer surface of the virus. Notably, we identified an interaction between the substrate-binding domain of heat shock protein family A member 5, an entry receptor for four related flaviviruses, and the hinge region of the viral envelope protein. We also identified host proteins involved in endocytosis, cytoskeletal rearrangement, or located in the cytoskeleton, suggesting that entry mechanisms for tick-borne encephalitis virus could include both clathrin-mediated endocytosis and macropinocytosis. Additionally, cross-linking of the viral proteins showed that the capsid protein forms dimers within tick-borne encephalitis virus, as previously observed with purified C proteins for other flaviviruses. This method enables the identification and mapping of transient virus-host interactions, under near-physiological conditions, without the need for genetic manipulation.

Author summary

Tick-borne encephalitis virus is an important human pathogen that can cause severe infection often resulting in life-long neurological complications or even death. As with other viruses, it fully relies on the host cells, and any successful infection starts with interactions between the viral structural proteins and cellular surface proteins. Mapping these interactions is essential both for the fundamental understanding

of viral entry mechanisms, and for guiding the design of new antiviral drugs and vaccines. Here, we stabilise the interactions between tick-borne encephalitis virus and human proteins by chemical cross-linking. We then detect the interactions using mass spectrometry and analyse the data to identify protein-protein complexes. We demonstrate that we can visualise the protein interaction interfaces by mapping the cross-linked sites onto the host and viral protein structures. We reveal that there are eight distinct sites on the outer surface of the viral envelope protein that interact with host. Using this approach, we mapped interactions between the tick-borne encephalitis virus envelope protein, and 59 host proteins, identifying a possible new virus receptor. These results highlight the potential of chemical cross-linking coupled with mass spectrometry to identify and map interactions between viral and host proteins.

Introduction

Viruses are obligatory intracellular parasites that depend on virus-host protein-protein interactions (PPIs) to establish successful infections. The identification of these interactions and knowledge of the interaction interfaces contribute to our understanding of the initial steps of the viral life cycle, and can guide the design of antivirals and vaccines [1–6].

Advances in high throughput methods have led to the large-scale identification of virus-host interactions, but the structural characterisation of these interactions is often still limited [7]. Affinity purification coupled with mass spectrometry, yeast two-hybrid, and protein microarrays, have identified virus-host PPIs for multiple viruses including: Japanese encephalitis virus, H1N1 influenza, human immunodeficiency virus, human cytomegalovirus, and severe acute respiratory syndrome coronavirus 2 [8–12]. These methods are however limited in their applicability to detect transient interactions between wild-type viruses and cells. Alternative methods, using chemical cross-linking, or proximity labelling (BioID and TurboID), demonstrate improved detection of weak and transient interactions [13–17]. In these approaches, cells are probed with modified viral proteins conjugated to trifunctional cross-linkers or biotin ligases. Host proteins in close proximity to the viral bait are then permanently cross-linked or biotinylated, and purified using the biotin or cross-linker tag. Enriched proteins are detected by comparison of the protein signal to that in negative

controls using bottom-up proteomics. Alternative chemical cross-linking mass spectrometry (XL-MS) workflows that directly detect the cross-linked peptides additionally provide information about the interaction interfaces. Previous studies have used the finite length of the chemical cross-linker to indicate the proximity of two amino acid side chains during the cross-linking reaction, and to build structural models of bacteria-host PPIs [18,19]. This shows the potential of XL-MS in both the identification of PPIs and the characterisation of the binding interface.

The flavivirus, tick-borne encephalitis virus (TBEV) is the causative agent of one of the most important arbovirus-caused diseases in Europe, Russia, and Northern China [20,21]. Symptomatic infection with TBEV can cause meningitis, encephalitis, and meningoencephalitis, and often results in life-long neurological complications or death [22,23]. The TBEV virion has three different structural proteins, the envelope protein (E protein), membrane protein (M protein) and capsid protein (C protein), in addition to a lipid bilayer and an ~11 kilobase-long positive-strand RNA genome (Fig 1). The E protein forms the smooth outer surface of the virion and is responsible for receptor binding [25,26]. The atomic structure of the mature TBEV virion E and M proteins has been solved by cryo-electron microscopy at a resolution of 3.9 Å and the crystal structure of the E protein at a resolution of 1.9 Å (Fig 1) [24,25]. Non-infectious immature and partially immature viruses also egress from cells, and have a spikey surface (Fig 1) [24]. No proteome-wide study of TBEV virus-host protein interactions has been published to our knowledge.

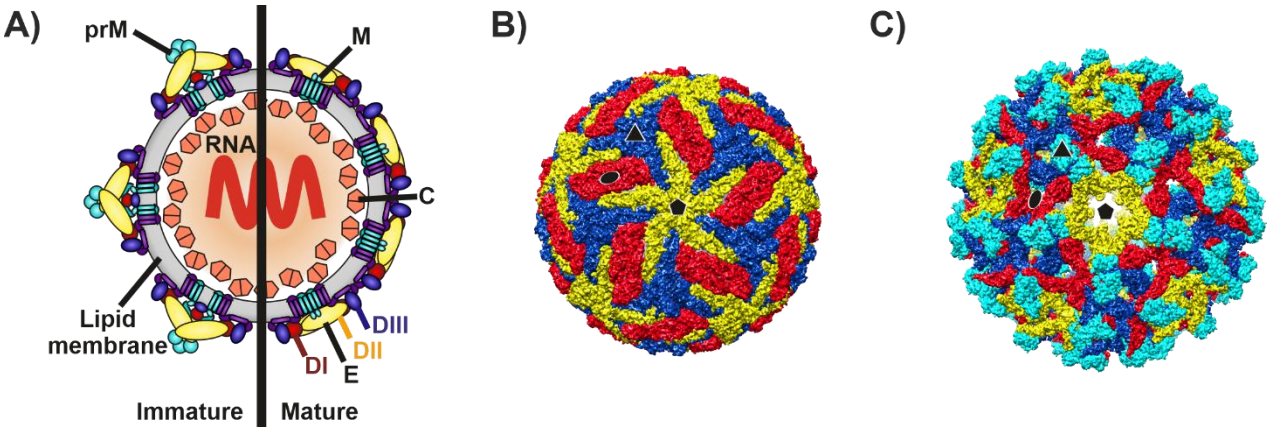

Fig 1: TBEV mature and immature virus structures. *A) Schematic representation of TBEV with the immature structure shown on the left and the mature on the right. Multiple copies of the C protein dimer*

surround the genome forming the nucleocapsid complex, positioned beneath the lipid bilayer. The surface of the immature virion is covered in 60 spikes, composed of trimers of prM (pre-membrane)-E heterodimers embedded into the lipid bilayer. The surface of the mature virion is covered in 90 E-M heterotetramer complexes embedded into the lipid bilayer. TBEV E protein domain I is shown in red, domain III in dark blue, domain II in yellow and domain 4 in purple. B) Surface representation of the mature TBEV virion (PDB accession: 5O6A)[24]. The three E proteins within each asymmetric unit are shown in blue, red, and yellow. Symmetry axes are indicated by the black pentagon (five-fold), triangle (three-fold), and ellipse (two-fold). C) Surface representation of the immature Spondweni virus, a related flavivirus (PDB accession 6ZQW) [27]. The three E proteins within each asymmetric unit are shown in blue, red, and yellow, and the prM protein is shown in cyan. Symmetry axes are indicated by a black pentagon (five-fold), triangle (three-fold), and ellipse (two-fold).

In this large-scale proteomics study, we used XL-MS to identify the interaction interfaces of PPIs between TBEV and the surface of human neuroblastoma (SK-N-SH) cells. Here, the homobifunctional chemical cross-linker disuccinimidyl suberate (DSS) was used to covalently fix PPIs by cross-linking primary amine containing residues (the side chain of lysine residues or the N-terminus of the protein). The finite length of DSS (11.4 Å) imposed a maximum distance between cross-linked residues and was used to validate intraviral crosslinks by measuring their distances on TBEV proteins with known structures or reliable homology models. The final dataset was filtered using the intraviral cross-links as an internal control, leading to the identification 59 unique high confidence interactions between the TBEV E protein and cellular proteins.

Results

Identification of cross-linked peptides

To identify interactions between the mature TBEV virion and host proteins, we incubated the virus with metabolically-stalled neuroblastoma cells on ice, allowing for TBEV to bind to the cells, but preventing

112 subsequent internalization. The TBEV-host PPIs were then stabilized and fixed by chemical cross-linking
113 with DSS (Fig 2). To reduce the sample complexity and search space during data analysis, we used limited
114 proteolysis to release primarily cell-surface associated host proteins. The released proteins were digested
115 to peptides and analysed by liquid chromatography tandem mass spectrometry (LC-MS/MS) followed by
116 label-free data dependent acquisition (DDA) quantitation to determine their relative abundance (S1 Table).
117 Identified proteins were used to generate smaller, defined sets of sequences to use in the cross-linking data
118 analysis workflow.

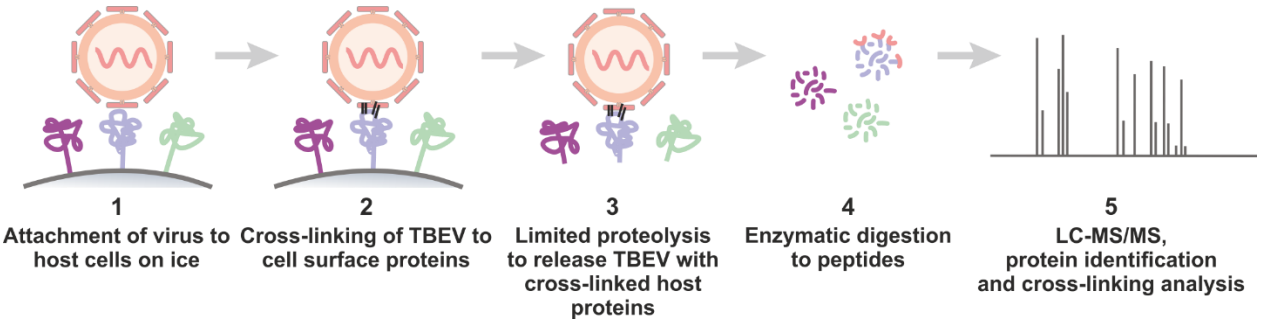

119

120 ***Fig 2: Schematic representation of cross-linking workflow.*** *1. TBEV was allowed to attach to metabolically-*
121 *stalled SK-N-SH cells. 2. TBEV-host PPIs were stabilised by chemical cross-linking with DSS. 3. Cell-surface*
122 *associated proteins, and cross-linked TBEV were released from the cell surface using limited proteolysis. 4.*
123 *The released proteins were digested to peptides. 5. Peptides were analysed by LC-MS/MS and host and viral*
124 *proteins identified and quantified using label-free DDA. Identified host proteins were analysed to identify*
125 *cross-links between the host proteins and TBEV.*

126 For cross-linking, we used four different cross-linker concentrations, in addition to a negative control
127 sample to which no cross-linker was added. Each condition was repeated in triplicate, and the experiment
128 repeated three times independently with different TBEV preparations and cell line passages, yielding 9
129 replicates per cross-linker concentration. The samples were initially analysed by immunoblotting of the
130 TBEV E and C Proteins (Fig 3). The presence of higher molecular weight bands greater than 100 kDa in
131 samples treated with DSS confirms cross-linking (Fig 3). The C protein has been shown to form antiparallel
132 dimers in the crystal and NMR structures of other flaviviruses [29–31]. We identified a band with a

133 molecular weight corresponding to that of C protein dimers, indicating that the C protein dimerizes in TBEV
134 (Fig 3).

135

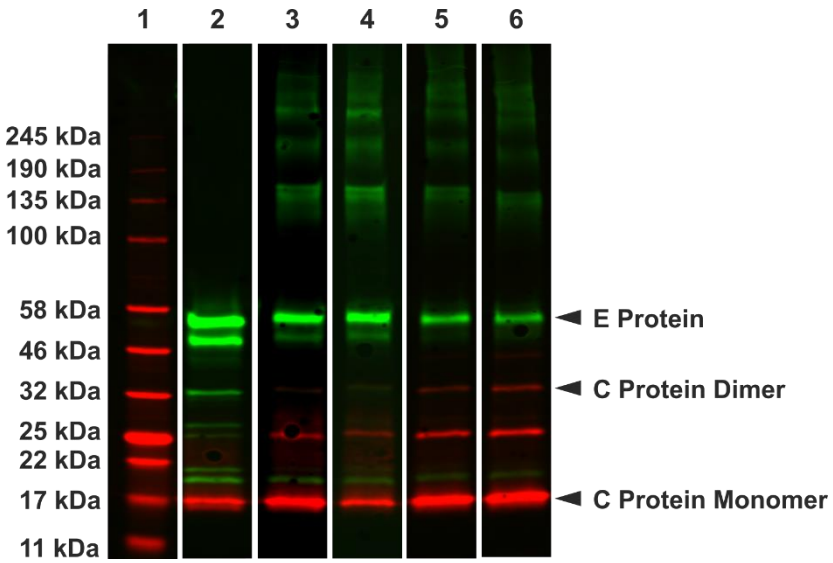

136

137 ***Fig 3: Immunoblot analysis of the TBEV E and C proteins in cross-linked samples.*** *The TBEV C protein in*
138 *shown in red and the TBEV E protein in green. Lane 1- protein marker; Lane 2- negative control with 0 mM*
139 *DSS, Lane 3- cross-linking with 0.1 mM DSS; Lane 4- cross-linking with 0.25 mM DSS; Lane 5- cross-linking*
140 *with 0.5 mM DSS; Lane 6- cross-linking with 1mM DSS. Higher molecular weight bands greater than 100 kDa*
141 *corresponding to the cross-linking of E and C to other proteins can be seen in lanes 2-5. Lower molecular*
142 *weight bands less than 50 kDa corresponding to the partial cleavage of the viral proteins during the limited*
143 *proteolysis step are also observed in all lanes.*

144 Identification of cross-linked peptides is computationally challenging as all primary amine-primary amine
145 combinations in a given sequence database need to be considered. To reduce the search space for cross-
146 linked peptide identification, proteins identified by DDA were probed for cross-links in batches (see
147 materials and methods). A total of 7167 spectral observations of cross-linked peptides were identified using
148 pLink2 at a false discovery rate (FDR) of 5%, excluding interfaces supported by cross-linked peptides
149 identified in the negative controls, which correspond to false positives likely arising from erroneous peptide
150 matches in the complex proteome background (S2 Table) [28]. Spectral observations of cross-links between

two peptides within the same protein (intraprotein PPIs) accounted for the majority of the observations (5589), compared to 1578 for those identified between two peptides from different proteins (interprotein PPIs). Intraprotein cross-links have been consistently shown to make up a higher proportion of spectral observations within cross-linked datasets, as two residues within the same protein are highly likely to be in close physical proximity within the cell, leading to an increased cross-linking frequency [32,33]. In total, 1697 different cross-linked interfaces were observed, and on average each interface was supported by 4.2 spectral observations. The cross-linked interfaces map to a network of 698 PPIs, consisting of 588 host proteins and the 3 viral structural proteins. Overall, 66.3 % of the unique PPIs were attributed to interactions between host proteins, 33.5 % to virus-host interactions and only 0.2 % to intraviral interactions. We also identified intraprotein cross-links in 297 host proteins and the TBEV C and E proteins.

The confidence of the cross-linking dataset can be investigated by examining the spatial distances between cross-linked residues for protein complexes where high-resolution structures or reliable homology models are available. As intraviral protein interactions account for 62 % of the detected spectral observations, we used the intraviral cross-links as an internal control to assess the confidence level for the dataset.

Mapping of intraviral cross-links

The published mature TBEV structure and homology models of the immature virus and C protein dimer were used to accurately measure cross-link distances. The C-score of the homology models were -0.65 (C protein), 2.00 (E protein) and 0.57 (prM protein) [34–36] . We measured the distance between cross-linked residues and applied a maximum distance constraint of 30 Å between the lysine or N-terminus Cα (Table 1 and Figs 1 and 4) [37]. In total, 24 cross-links were mapped onto the viral structural proteins, and 22 fell within the accepted distance range. Overall, 14 of the cross-links satisfied the distance constraint in both the mature and immature TBEV structures, six were only acceptable in the mature structure and two in the immature structure. Cross-links with acceptable distances in only the mature structure were identified by 2089 spectral observations compared to 31 for those only accepted in the immature structure, demonstrating that the majority of the virus particles in the analysed samples were mature.

176 **Table 1: Intraviral cross-links identified, the corresponding average expectation value and SVM score of**

177 **the peptide spectrum matches, and distances in the mature and immature virus structures**

Cross-link Type	Protein 1	Protein 2	Residue 1*	Residue 2*	Mean E-Value	Mean SVM Score	Number of Spectral observations	Distance Between Cα Carbons Virion	Distance Between Cα Carbons Immature Virus
Intradimer/ Intertrimer	E Protein	E Protein	251	284	0.59	0.07	1346	16.74	47.74^
Intramonomer	E Protein	E Protein	64	126	0.25	0.08	939	12.10	11.95
Intramonomer	E Protein	E Protein	300	161	0.02	0.02	910	17.42	15.99
Intramonomer	E Protein	E Protein	118	69	0.13	0.11	315	9.47	9.08
Interdimer/ Intertrimer	E Protein	E Protein	136	309	0.48	0.10	265	17.25	32.41^
Interdimer/Intertrimer	E Protein	E Protein	309	69	0.09	0.10	172	17.88	30.87^
Intradimer	E Protein	M Protein	266	1	0.42	0.15	155	8.79	N/A
Interdimer/ Intertrimer	E Protein	E Protein	118	309	0.34	0.06	150	18.54	30.67^
Intramonomer/ Intradimer	C Protein	C Protein	10	25	0.41	0.06	63	23.18/23.68	23.18/23.68
Intramonomer	E Protein	E Protein	64	69	0.35	0.16	34	15.26	14.58
Interdimer/ Intertrimer	E Protein	E Protein	251	311	1.00	0.03	23	31.63^	28.63
Intramonomer/ Intradimer	C Protein	C Protein	20	10	0.09	0.02	19	16.45/24.22	16.45/24.22
Intramonomer/ Intradimer	C Protein	C Protein	20	8	1.00	0.35	12	19.30/28.73	19.30/28.73
Interdimer/Intertrimer	E Protein	E Protein	251	309	1.00	0.03	10	26.00	29.38
Intramonomer	E Protein	E Protein	251	69	1.00	0.03	9	9.11	8.26
Interdimer/ Intertrimer	E Protein	E Protein	64	161	1.00	0.06	8	39.39^	30.06
Interdimer/Intertrimer	E Protein	E Protein	64	309	1.00	0.30	4	25.91	27.17
Intramonomer	E Protein	E Protein	309	407	1.00	0.41	3	41.09^	43.78^
Intramonomer	C Protein	C Protein	20	25	0.69	0.22	3	7.12/32.63^	7.12/32.63^
Intramonomer	E Protein	E Protein	309	408	1.00	0.50	2	39.54^	41.45^
Intramonomer	E Protein	E Protein	69	124	1.00	0.62	1	26.85	25.98
Intramonomer	E Protein	E Protein	298	309	1.00	0.23	1	25.96	26.46
Intramonomer	E Protein	E Protein	311	309	1.00	0.22	1	6.04	5.60
Interdimer	M Protein	M Protein	1	1	1.00	0.70	1	19.70	N/A

178 *The TBEV polyprotein sequence was obtained from GenBank (accession: AWC08512.1). The C protein corresponds to

179 residues 1-96; the M protein 206-280 and the E protein 281-776. Residue numbers in the table begin from 1 at the

180 start of each protein.

181 ^Distances between cross-linked residues that are greater than 30 Å and are not considered feasible.

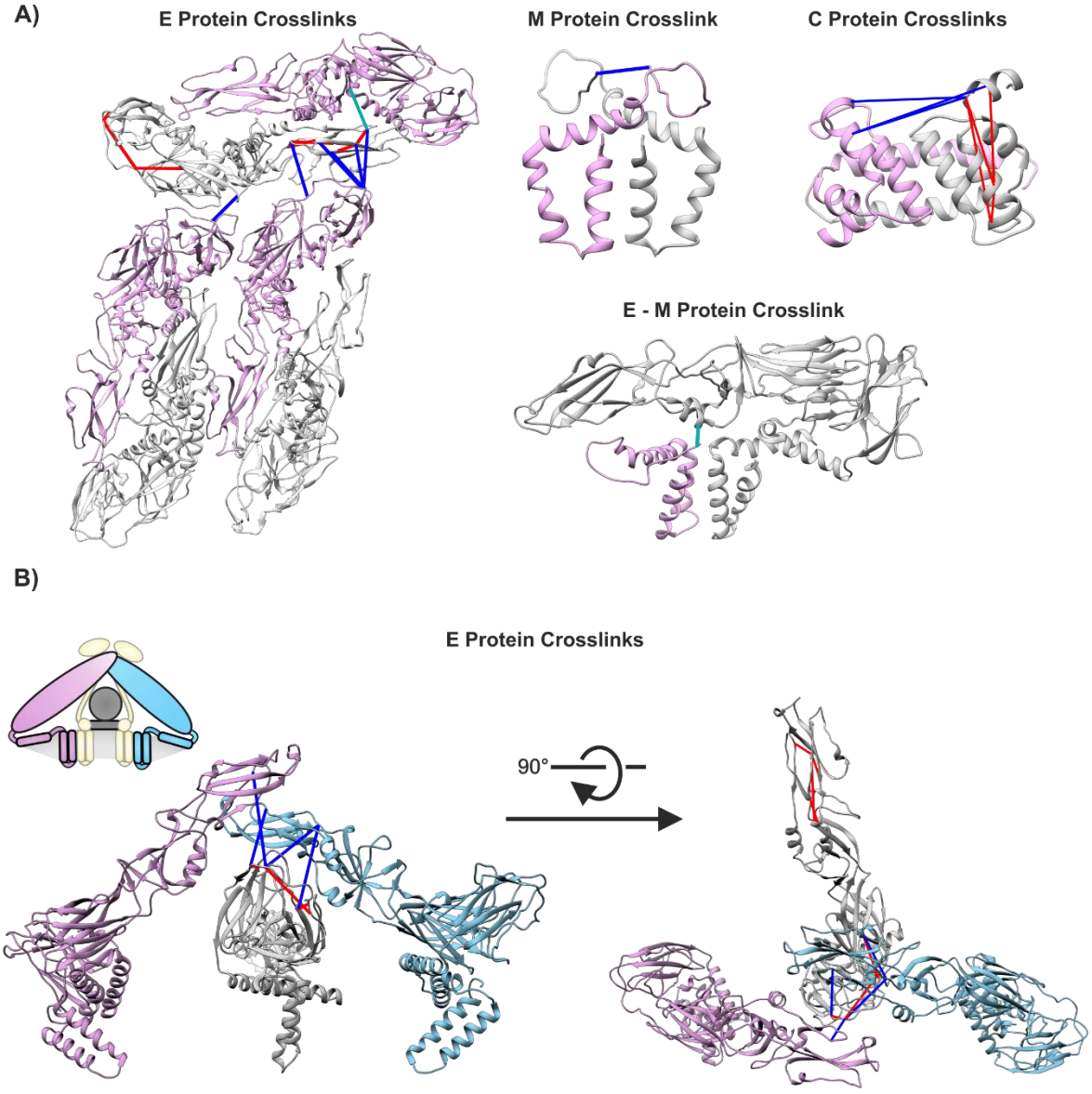

Fig 4: Mapping of intraviral crosslinks. *Identified intraviral cross-links with the distances ≤ 30 Å mapped to the viral structural proteins are shown above in red, blue and teal. Red cross-links corresponding to intramonomer cross-links, teal intradimer cross-links, and blue interdimer or intertrimer cross-links. A) Cross-links mapped to the known cryoEM structure of the TBEV virion or the C protein homology model. B) Cross-links mapped to the generated homology model of the immature virus, E proteins in trimer 1 are coloured in plum and light blue and the E protein in trimer 2 is coloured grey. The schematic diagram additionally shows the position of the lipid bilayer (light grey) and the prM protein (light yellow).*

Locating the cross-links on the virus structures with distance constraints applied, allowed us to distinguish between three different types of E-E cross-links in the mature virion: intramonomer, intradimer and

192 interdimer cross-links, and two in the immature virus: intramonomer and intertrimer cross-links. As
193 expected, intramonomer E cross-links show similar distances in the mature and immature structures and
194 accordingly the distance constraints are satisfied equally well for both. In contrast, as the E proteins
195 rearrange from trimers to dimers upon virus maturation, only 2 cross-links satisfy the distance constraint in
196 both the intertrimer positions found in the immature virus and the intradimer or interdimer positions
197 found in the mature virus. Two types of cross-links are possible within the C protein dimer, intramonomer
198 and intradimer. In our dataset, three of the four identified C protein cross-links satisfy the distance
199 constraints for both interaction types, making it impossible for us to distinguish between these two
200 alternatives.

201 Two of the intramonomer cross-links between E protein residues 309 and 407 or 408 demonstrate cross-
202 linking lengths of ca. 40 Å in both the mature and immature structures. The cross-links were identified by a
203 low number of spectral observations, 3 for 309-407 and 2 for 309-408, and may arise from interactions
204 between disrupted virions, free E proteins, alternative viral conformations or be false positives. To
205 distinguish between these alternatives, we examined the cross-linked spectra in detail (Fig 5). Fig 5A shows
206 representative spectra for cross-links that satisfy the distance constraint and are identified by a high
207 number of spectral observations, and Fig 5B and C show representative spectra for the two questioned
208 crosslinks. As compared to the spectra shown in Fig 5A, spectra in Fig 5B and C show both a low signal-to-
209 noise ratio and a low sequence coverage for the peptide fragments, and most likely represent false positive
210 hits from background noise.

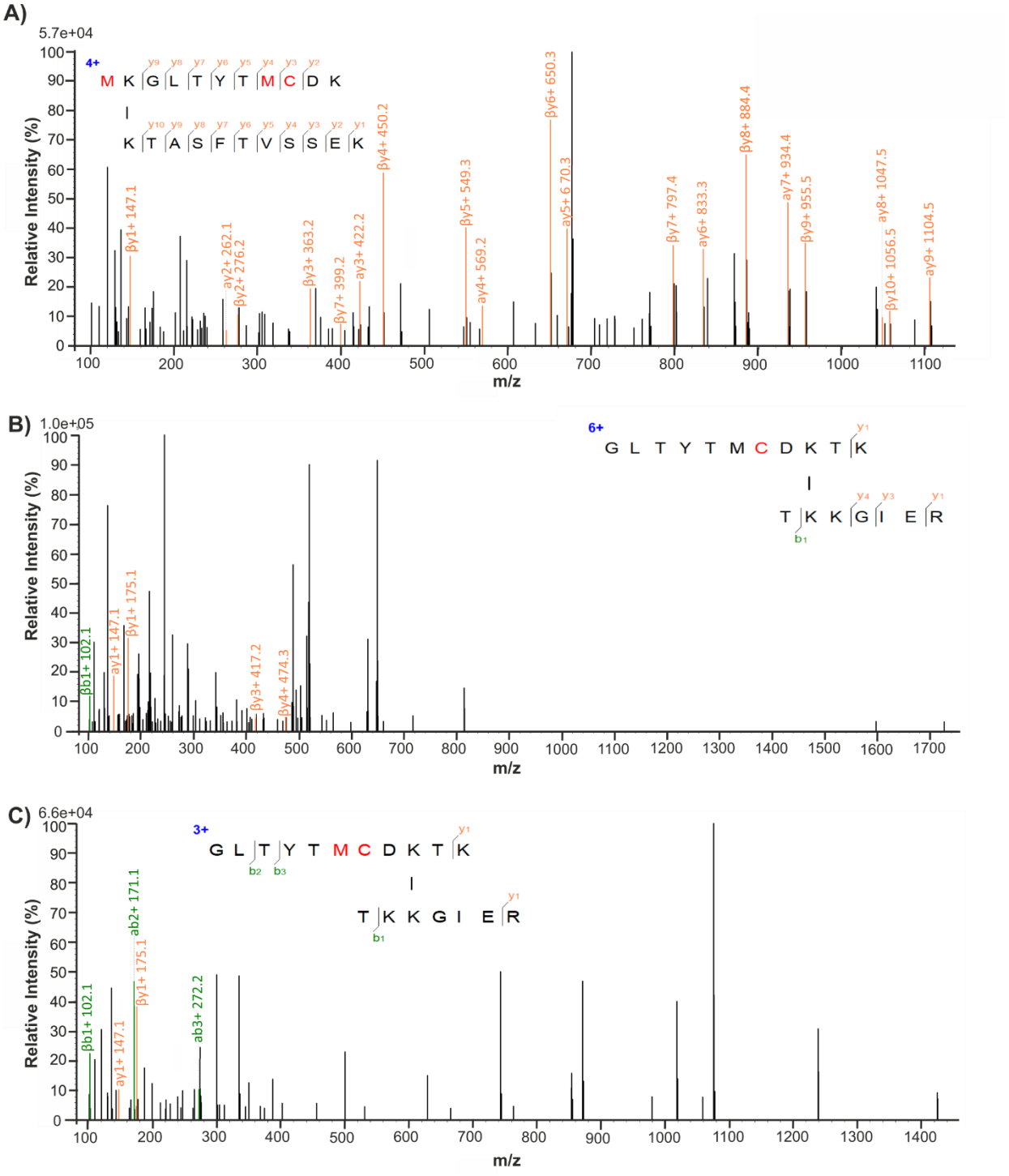

211

212 ***Fig 5: Representative spectra of E protein cross-links that satisfy the distance constraint (< 30 Å) and***

213 ***cross-links with distances > 30 Å.*** *The cross-linked peptides are shown with the longer α peptide positioned*

214 *above the shorter β peptide and a connecting line between the cross-linked residues. Modified residues in*

215 *the peptides are shown in red and the detected beta and gamma fragments shown in green and orange*

216 *respectively. Peaks corresponding to the detected fragments are coloured and labelled accordingly. The*

charge state of the cross-linked peptide is shown in blue. A) Representative spectrum of E protein cross-link 300-161 that are less than 30 Å and show a high number of spectral observations. B) Representative spectrum for the cross-link 309-407, that has a cross-linking distance of 41.09 Å in the mature structure and 43.78 Å in the immature structure. C) Representative spectrum for the cross-link 309-408 that has a cross-linking distance of 39.54 Å in the mature structure and 41.45 in the immature structure. Cross-links with distances > 30 Å show poor fragmentation and signal to noise ratio in the cross-linked spectral (B and C), compared to cross-links with distances < 30 Å (A).

Based on the imposed distance constraints, we calculated that 91.7 % of the intraviral cross-linked interfaces are identified with high confidence, at a distance threshold of <30 Å indicating that our approach allows detection of specific intra- and inter-protein cross-links with high confidence.

Filtering the cross-linking dataset

The program pLink2 provides two parameters for assessing the confidence of cross-linked peptide spectrum matches (PSM), the expectation value (E-value) and the SVM score [28]. Both the E-value and SVM score describe the probability of a cross-linked PSM being a random match, and have values ranging from 1 to 0, where the smaller the value the more confident the PSM. The SVM score is calculated for every PSM, acting as the prime measure for FDR estimation, whereas the E-value is only calculated for PSMs that pass the FDR threshold [28]. In addition, cross-links may occur due to the sporadic proximity of proteins in the sample, or due to specific cross-linking of interacting proteins. Cross-links identified by more spectral observations have a higher probability of reflecting specific interactions. Therefore, the number of spectral observations per cross-linked interface can provide information about the cross-linking confidence on the protein-protein interaction level. Previous studies have used the E-value, SVM score, number of spectral observations or a combination of the aforementioned to assess the confidence of the identified cross-links but no standardized values have been established [28,38,39]. Here, we investigated the correlation between the E-value, SVM score, number of spectral observations and the acceptable distance constraint (<30 Å) as measured for our intraviral cross-links, to determine confidence parameters for the dataset.

Our data show a correlation between the measured distance of each unique intraviral cross-link and the calculated SVM scores, but not the E-values (Fig. 6, S1 Fig). Consequently, the E-value was not considered as a suitable measure of confidence for this dataset. We observed that intraviral cross-links with distances > 30 Å in both the mature and immature structures (indicated as red bars in Fig. 6) had the 3rd and 4th highest mean SVM scores of the intraviral cross-links (Table 1). Furthermore, cross-links with higher mean SVM scores were only identified by one spectral observation (Table 1). Based on the SVM scores of intraviral cross-links with distances > 30 Å in both the mature and immature structures, we imposed a SVM score threshold of < 0.355, hence discarding 884 of the identified cross-linked interfaces. Interestingly, 97.8 % of the excluded interfaces were identified by only one spectral observation.

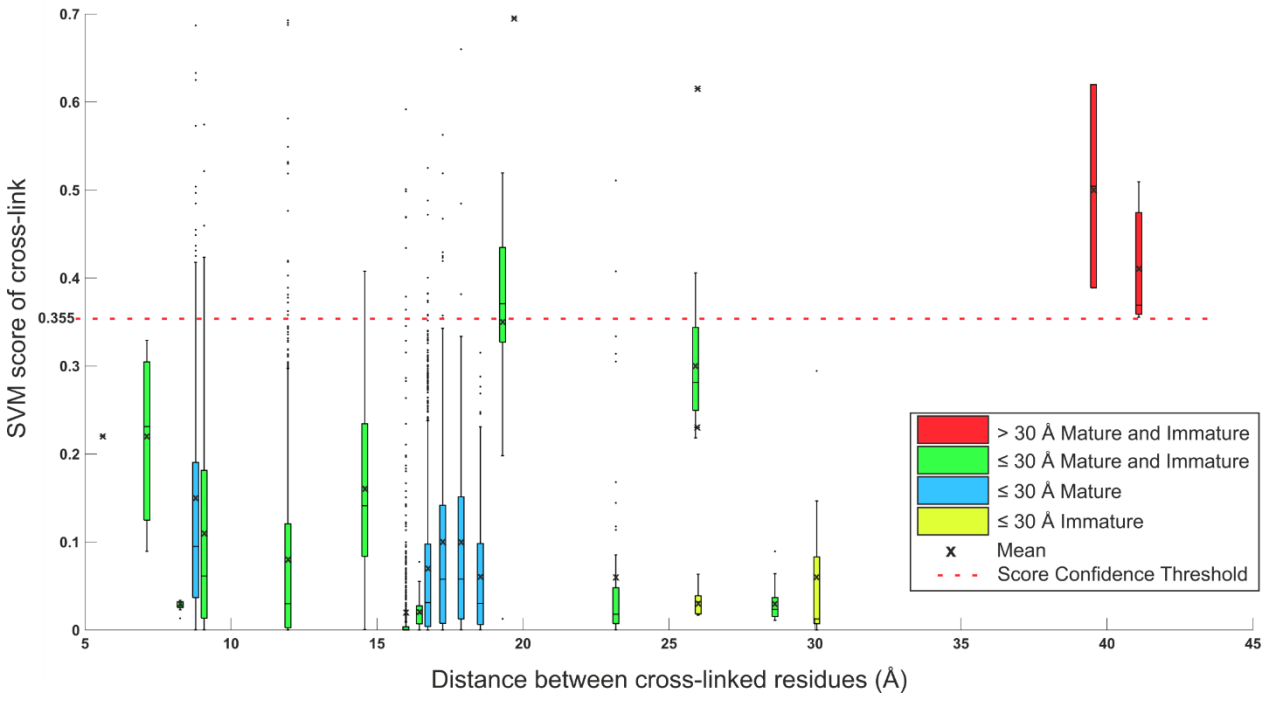

Fig 6: Box and whisker plot of the SVM scores for the intraviral cross-links, plotted against the distance between the cross-linked residues for each cross-link. *The bars are coloured based on whether the distance constraint is satisfied for both the mature and immature conformations (green), only the mature conformation (blue), only the immature conformation (yellow) or not satisfied in either the mature or immature conformation (red). The mean SMV score is marked with a cross. A SVM score confidence threshold of < 0.355 is shown by a red dashed line.*

The number of cross-linked spectral observations for 101 randomly selected proteins in the dataset was compared to the average spectral count of these proteins across all the samples in the DDA analyses (S1 File). The number of spectral observations for cross-linked peptide pairs for these same 101 selected proteins was also compared to the number of lysine residues present within each protein (S1 File). No correlation was observed in either of these cases; so, neither protein abundancy nor lysine content affect the data content (S1 File). Therefore, the number of spectral observations was used in a non-biased manner to assess the confidence of each unique cross-link to reduce the dataset for analysis further.

Here, we filtered the data in a stepwise manner, first on the PSM level using the SVM score and secondly on the protein-protein interaction level using the number of spectral observations. A cross-linked interface was considered to be of high confidence if it had an SVM score < 0.355 and was identified by ≥ 2 spectral observations. Filtering the data in the reverse order would lead to inclusion of interactions only supported by one high confidence spectral observation. The filtered cross-linking dataset consisted of 218 cross-linked interfaces, 36.7 % of which were attributed to virus-host PPIs (S3 Table).

Virus-host protein-protein interactions

Virus-host PPIs were identified between TBEV and 61 host proteins in the filtered cross-linking dataset. In total, 59 proteins were shown to interact with the TBEV E protein and 2 with the M protein. Cross-links with the M protein form between N-terminal serine of mature M and the host proteins. As the M protein is buried and not accessible for cross-linking in the mature virion, these interactions likely occur between the host proteins and disrupted virions, free M protein, or conformations that have yet to be described.

E -host PPIs were mapped to eight different lysine residues on the outer surface of the virion (E protein residues 118, 126, 136, 161, 251, 280, 300, and 336; Fig 5), indicating that the host proteins were indeed interacting with assemble capsids. Only six of these residues shown in blue are also accessible on the outer surface of the immature particle, as residue 336 is obscured by other E proteins and residue 251 by prM (Fig 7). The cross-linked lysine residues are distributed evenly across the surface of the E protein, showing no preference for domains I, II or III (Fig 7).

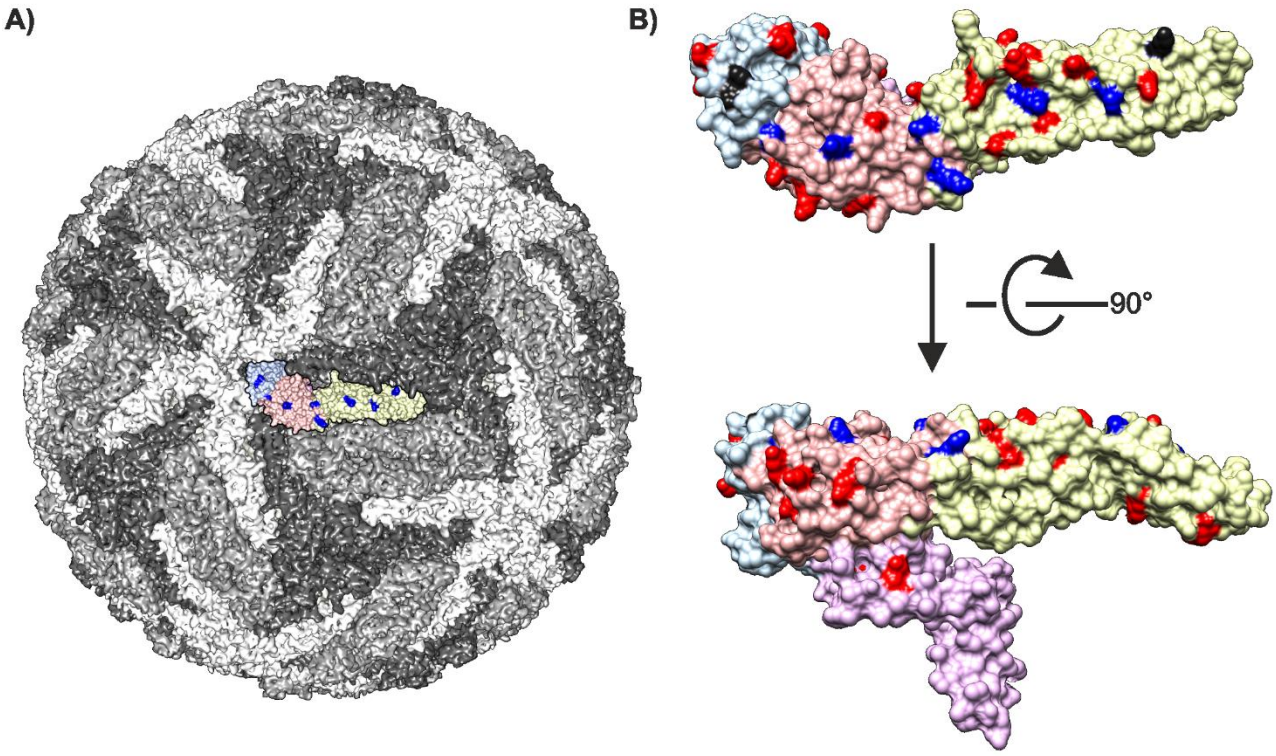

Fig 7: Visualisation of E protein lysine residues that form cross-links with host proteins. *A) Surface representation of the TBEV virion (PDB accession: 5O6A) [24]. The three E proteins within each asymmetric unit are shown in white, grey and dark grey. One E protein monomer is shown in colour (TBEV domain I is shown in peach, domain II in yellow, domain III in lilac with the cross-linked lysines shown in blue. B) Mapping of the cross-linked lysines on the structure of the E protein (PDB accession 5O6A). Lysines detected with cross-links are shown in blue if located on the surface of both the mature and immature virus and black for those only located on the surface of the mature virus; lysines without cross-links are shown in red. TBEV domain I is shown in peach, domain II in yellow, domain III in light blue and domain IV in lilac.*

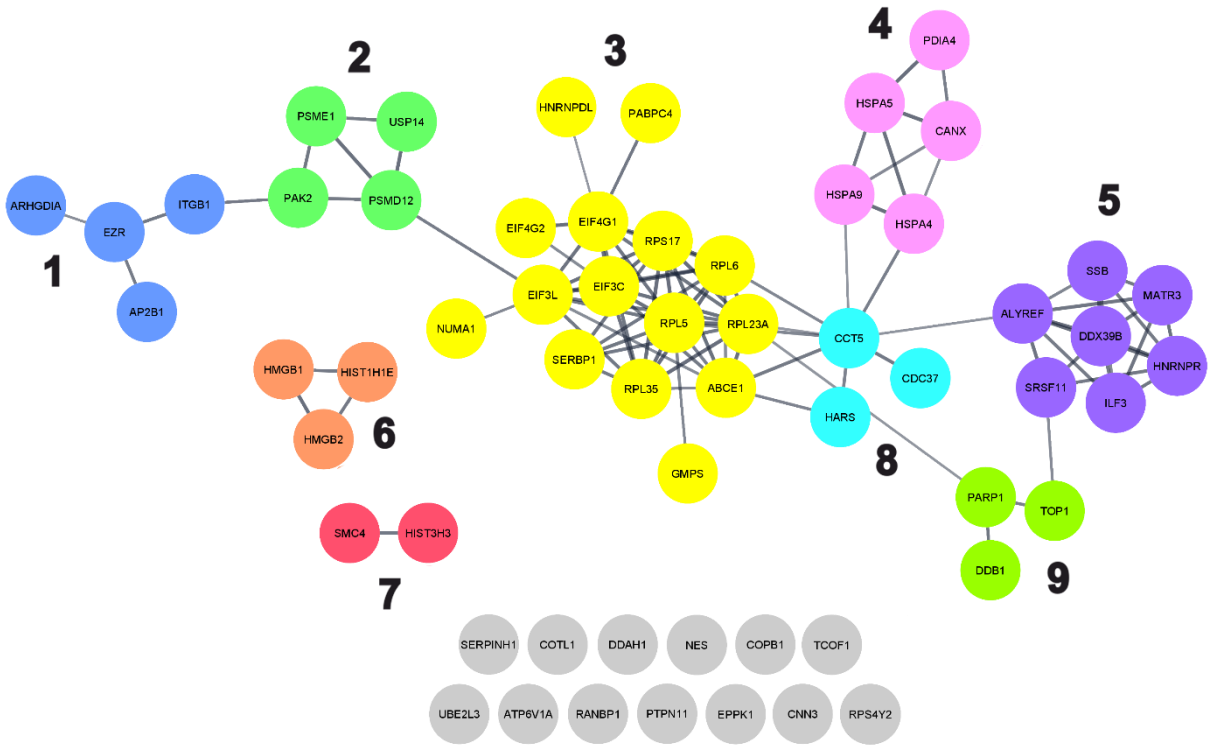

Fig 8: String network of 59 host proteins identified as interacting with the TBEV E protein in the filtered cross-linking dataset. *The string-database network shows both direct and indirect protein interactions and is clustered based on the combined score associated with each interaction, using the Markov clustering algorithm [40]. Proteins are coloured based on the clustering and each cluster is numbered (1-9). Proteins that do not have any known interactions with other host proteins identified in the filtered cross-linking dataset are shown in grey.*

We performed String-database analysis to identify if any of the 59 E protein-interacting host proteins also interact with each other (Fig 6) [40]. In total, 46 proteins were shown to interact with at least one other protein, and nine interaction clusters were identified. This suggests that TBEV may interact with both individual proteins and larger protein complexes. Gene ontology (GO) analysis (S4 Table) of the clusters indicates that proteins in clusters 1, 2 and 4 are located in the extracellular region (GO:0005576), at the plasma membrane (GO:0005886) or in extracellular exosomes (GO:0070062). Clusters 1 and 2 show enrichment for receptor-mediated biological processes, including receptor-mediated endocytosis (GO:0006898; cluster 1), and receptor-mediated signalling (GO:0038095, GO:0050852, GO:0002223; cluster

2), whereas proteins in cluster 4 are involved in protein transport (GO:0015031). Cluster 3 is the largest cluster and consists of proteins found in the cytosol (GO:0005829) predominantly as part of ribosomes (GO:0005840), ribonucleoprotein complexes (GO:1990904) or the eukaryotic translation initiation factor 4F complex (GO:0016281). Other cytosolic proteins belong to cluster 8 (GO:0005829) and are involved in protein folding (GO:0006457) or translation (GO:0006412). Finally, proteins in clusters 5, 6, 7 and 9 are primarily found in the nucleus (GO:0005634) and are involved in RNA processing (GO:0006396), posttranscriptional regulation of gene expression (GO:0010608; cluster 5), and chromosome organisation (GO:0051276; clusters 6, 7 and 9). Importantly, many proteins primarily located in the cytosol or nucleus (clusters 3, 5-9) are also found in the plasma membrane or extracellular regions where they perform alternative biological functions; for example, HMGB1 (UniprotKB:P09429; cluster 6), functions as a nonhistone nucleoprotein in the nucleus and an inflammatory cytokine in the extracellular region [41]. In addition, GO analysis identified 19 proteins that are associated with immune system process, and 11 proteins associated with the cytoskeleton or cytoskeletal rearrangement.

Discussion

In this study, we present a chemical cross-linking proteomics approach to simultaneously identify TBEV-neuroblastoma cell PPIs and their interaction interfaces. We used metabolically-stalled cells to adsorb and cross-link virus only to the cell surface, hoping to primarily enrich proteinaceous cell surface interactions. The cross-linked proteins were released by limited proteolysis. Analysis of this highly complex protein mixture by LC-MS/MS generated a large database of spectra containing four different peptide species with the minority being cross-linked. In addition, cross-linked peptides are the least well-fragmented in the database. In the next step, the pLink2 software compares the database of spectra with all of the possible theoretical cross-linker reaction outcomes. This step is a clear bottle neck in the process as in our hands, only 28 proteins could be analysed at a time, requiring multiple batch runs. Here, we optimised the analysis workflow in order to extract the most significant virus-host PPIs from our complex data. Firstly, we reduced the cross-linking search space by only analysing proteins identified by linear peptides in the samples.

Secondly, we have an internal validation control in the sample. We identified high-confidence intraviral crosslinks using both the known and predicted three-dimensional structures of TBEV and the known length of the chemical cross-linker. Then, we correlated the high confidence cross-links with the SVM score and the quality of the spectra, allowing us to use an SVM score cut-off < 0.355 for the entire dataset. Finally, we imposed a spectral count cut-off ≥ 2 to select for the most specific protein interactions. Using this method, we identified 22 high confidence unique intraviral cross-links and 59 high confidence unique virus-host PPIs between the surface of TBEV and human neuroblastoma cells. These proteins form a robust and reliable dataset that can be investigated further for their roles in the virus life cycle. They could be targets for intervention.

Our approach presents four major advantages over alternative approaches used to identify virus-host PPIs described in the literature: 1) The wild-type virus interacts with cellular proteins on the surface of neuroblastoma cells. In comparison, affinity purification, yeast two hybrid and protein microarrays detect interactions in artificial systems [8–12]. Therefore, the expression levels, presentation and glycosylation state of the host and viral proteins may differ from that in natural infections, leading to both false positives and false negatives; 2) When fully assembled viral particles are used as bait, the capsid proteins are in the right biological conformation and molecular context for infection. In contrast, single recombinant bait proteins used in affinity purification, yeast two hybrid, protein microarrays and BioID may not be [8–12,16]. For instance, the monomeric Dengue virus ancillary receptor, DC-SIGN binds across two neighbouring E proteins on the capsid [42]. In our virus-based protocol, there would be 90 such sites for the DC-SIGN interaction giving both the correct biological context, but also increasing the avidity of the interactions; 3) The virus interacts with cellular proteins prior to crosslinking. In contrast, in the previously described approaches using trifunctional cross-linkers or BioID, the viral proteins are first conjugated to the cross-linker or biotin ligase prior to the interaction with cells. Conjugation may require genetic modification [13–17]. Consequently, interactions may be missed if the modification sterically hinders the binding region. Here we could identify PPIs, under near-physiological conditions, without the need for genetic manipulation; 4) The clearest advantage in our approach is that we map virus-host PPIs directly from the

358 cross-linked peptides. This gives us additionally information about which residues are within 30 Å of each
359 other and form the interaction interface.

360 Although this approach shows promise for detecting a wide-range of virus-host PPIs, there are also some
361 challenges. The complete coverage of the interaction space is limited by the accessibility of surface cross-
362 linkable lysine residues and the sample complexity. In order to detect an interaction, there must be cross-
363 linkable residues on both sides of the interaction interface within 30 Å of each other. Furthermore, in
364 complex systems containing a higher number of protein species, the number of cross-links per species is
365 lower in comparison to simpler systems. Consequently, interactions that occur in lysine deficient regions or
366 with low frequency cannot be detected, leading to an incomplete picture of the interaction interface or
367 failure to detect the PPI. Performing parallel experiments using chemical cross-linkers with different lengths
368 or reactive residues such as arginine, aspartate or glutamate, could overcome this limitation [43,44]. Simple
369 cross-linking experiments including only the virus and a single interaction partner can be used to ensure
370 complete coverage of the 3D interaction space once interesting PPI have been identified.

371 Having considered the potential advantages and challenges of this protocol, we will now consider potential
372 biological implications. Laminin binding protein has previously been suggested as a TBEV receptor. It was
373 present in our dataset, but no cross-links were identified to TBEV [45,46]. Our data do not support that
374 laminin binding protein is a TBEV receptor in this cell line. However, we have identified proteins that are
375 associated with the early stages of viral infection in other viruses, including ITGB1, ATP6V1A, EZR, HSPA9,
376 and HSPA5. ITGB1 as an entry receptor for a large number of viruses including, cytomegalovirus, Epstein-
377 Barr virus, human parvovirus B19, and mammalian reovirus [47–50]. ATP6V1A directly interacts with rabies
378 viral matrix protein facilitating uncoating [51]. EZR is an essential host factor required for the entry of
379 Japanese encephalitis virus into human brain microvascular endothelial cells [52]. HSPA9 has been
380 identified as a putative receptor for Tembusu virus [53].

381 HSPA5 (Cluster 4, Fig 6) has been identified as a receptor for several flaviviruses including, Zika and
382 Japanese encephalitis where HSPA5 was shown to affinity purify with recombinant E protein domain III, but

383 the interaction context in virions has not been studied [55,56]. HSPA5 is a multifunctional regulator of
384 endoplasmic reticulum homeostasis, playing an important role in protein processing and quality control
385 [58–61]. It is located both in the endoplasmic reticulum lumen and on the outer surface of the plasma
386 membrane in many cell types including neurons [62–65]. HSPA5 consists of 2 domains, a nucleotide-binding
387 domain that binds ATP, and a substrate-binding domain that binds and stabilises partially folded or folded
388 proteins [66]. Here we identified four spectral observations mapping to the TBEV E hinge region (residue
389 136) and the HSPA5 substrate binding domain residues 521 and 516 (Fig 9). Therefore, the interaction
390 between HSPA5 and the E protein hinge region could constitute a unique binding interface, or be part of a
391 larger interface that also binds domain III consistent with other flavivirus studies [53–55,57]. We
392 hypothesize that HSPA5 could interact with both the hinge region of one E monomer and domain III of an
393 adjacent E monomer at the 3-fold axis, where the regions are in close spatial proximity (Fig 9).
394 Interestingly, Fab fragments of the TBEV neutralising antibody 19/1786 have been shown to bind across
395 this interface at the 3-fold axis potentially preventing the HSPA5 interaction[24]. Although, no cross-links
396 were detected between domain III and HSPA5 in our study, this can be partly explained by poor lysine
397 availability. Structural bioinformatics studies of the Zika virus domain III-HSPA5 interaction do not detect
398 any interacting lysine residues on HSPA5[67].

399

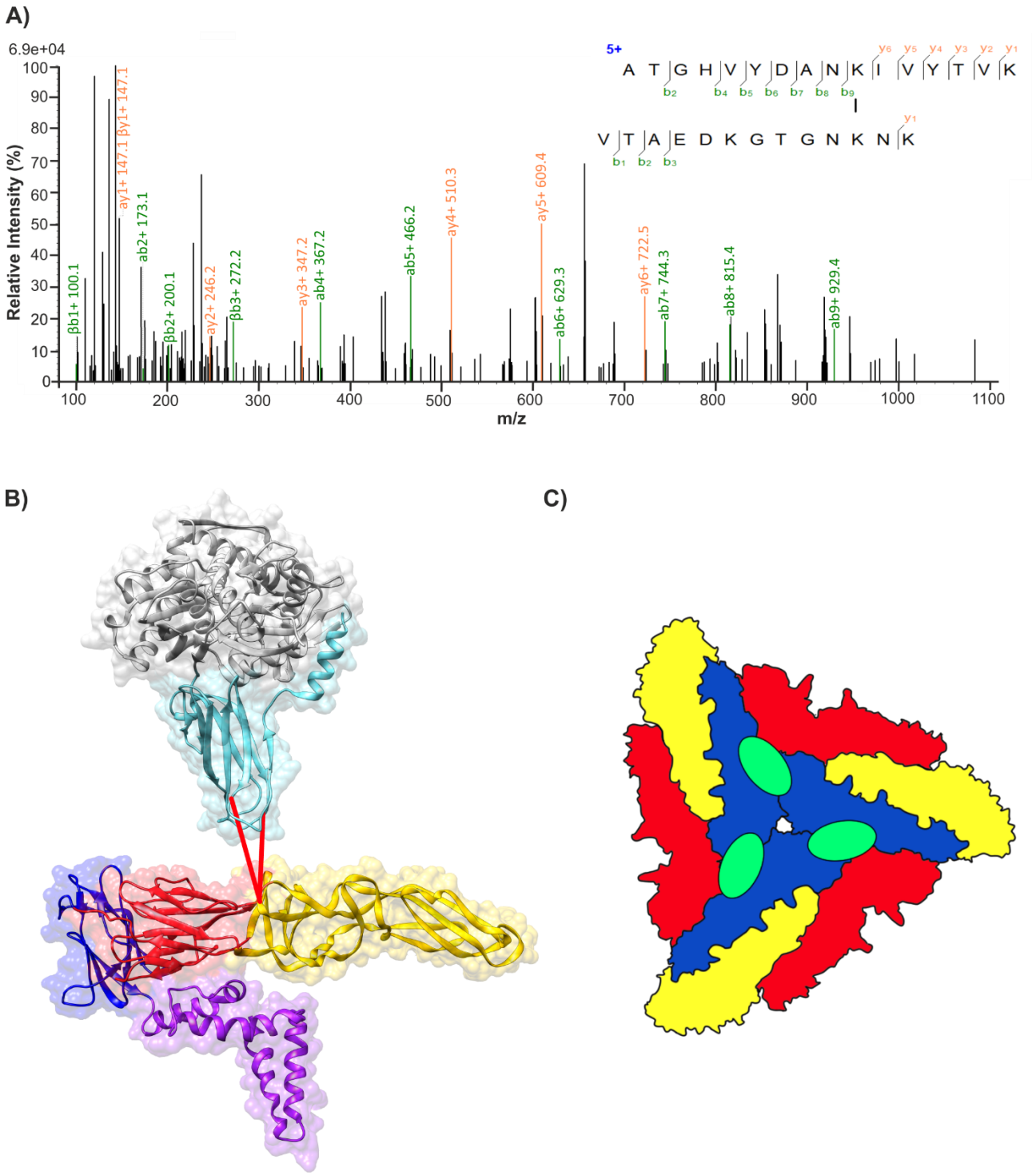

400

401 ***Fig 9: Cross-linking of HSPA5 and TBEV E protein*** *A) Assigned spectrum for the peptide associated with the*

402 *HSPA5-E protein interaction. B) TBEV E protein (PDB accession 5O6A) and HSPA5 (PBD accession 6ZMD)*

403 *were placed in close proximity to allow for the visualisation of the cross-links, indicated here with red lines.*

404 *TBEV E protein domain I is shown in red, domain III in dark blue, domain II in yellow and domain 4 in purple.*

405 *HSPA5 substrate-binding domain is shown in light blue and the remainder of the protein in grey. C)*

Schematic representation of speculated HSPA5 binding region on the mature virus. The three E proteins within each asymmetric unit are shown in blue, red, and yellow. The proposed HSPA5 binding site is shown in green.

After the virus has attached to the cell surface, the next step is to enter the cells either through clathrin-mediated endocytosis or macropinocytosis, and we found evidence for both pathways being used. We identified AP2B1 in the GO analysis that binds to the clathrin heavy chain [68]. We also identified an abundance of cytoskeletal proteins and cytoskeletal remodelling proteins required in macropinocytosis including, NES, NUMA1, ITGB1, EZR, PAK2, COTL1, CCT5, CNN3, EPPK1 and RANBP1. This supports the hypothesis that macropinocytosis is used by TBEV as well as Dengue virus [69].

Conclusions

In this study, we present a XL-MS method to identify and map transient virus-host PPIs under near-physiological conditions, without the need for genetic modification. Using this method, we identified 59 high confidence virus-host PPIs between TBEV and the surface of neuroblastoma cells. These proteins form a robust and reliable dataset that can be investigated further for functional relevance in targeted follow-up experiments. The presented methodologies are generally applicable to other virus-host systems and can assist in expanding our knowledge of viral infections.

Materials and methods

Viruses and cells

Neuroblastoma SK-N-SH cells (ECACC 86012802) were maintained in Dulbecco's modified Eagle's medium (DMEM) (Sigma) supplemented with 10 % heat inactivated FBS (Gibco), 100 µg/ml of penicillin-streptomycin mix (PenStrep) (Sigma) and 2 mM L-glutamine (Sigma), at 37 °C and under a 5 % CO_2 atmosphere. For virus propagation, cells were infected with TBEV strain, MG569938 Kuutsalo-14 *Ixodes ricinus* Finland-2017, at a MOI of 0.003, in Dulbecco's modified Eagle's medium (DMEM) (Sigma)

supplemented with 2 % heat inactivated FBS (Gibco), 100 µg/ml of penicillin-streptomycin mix (PenStrep) (Sigma), 2 mM L-glutamine (Sigma) and 0.35 µM rapamycin and incubated at 37 °C for 3 days under a 5 % CO_2 atmosphere. Virus-containing supernatant was aspirated and centrifuged at 4500 x g for 5 minutes to remove cell debris. Cleared supernatant was aliquoted into cryopreservation vials and frozen at -80 °C. Viral titers were determined using plaque-forming assay. SK-N-SH cells were grown on a 6-well plate, infected with ten-fold serial dilutions of the virus and incubated for 1 hour at 37 °C, under a 5 % CO_2 atmosphere. Overlay medium (Minimum Essential Medium Eagle, PenStrep and 2 mM L-glutamine, 1.2 % avicel) was added to each well and the cells incubated for 4 days at 37 °C, under a 5 % CO_2 atmosphere. After 4 days the cells were fixed with 10 % formaldehyde, stained with crystal violet and the plaques counted to determine the number of plaque forming units per ml (PFU/ml).

Production of amino acid free virus stock

SK-N-SH cells were grown to 90% confluence, washed twice with PBS and the medium changed to amino acid free DMEM (Genaxxon) supplemented with 100 µg/ml of penicillin-streptomycin mix (PenStrep) (Sigma) and rapamycin 0.35 µM (selleckchem). Cells were infected with TBEV, at multiplicity of infection 1, and incubated at 37 °C for 4 Days, under a 5 % CO_2 atmosphere. Virus-containing supernatant was aspirated and centrifuged at 4500 x g for 5 minutes to remove cell debris. The virus was pelleted through a 30 % sucrose cushion in HNE buffer (20 mM HEPES pH 8.5, 150 mM NaCl, 1 mM EDTA), 2 h, 27000 rpm, 4 °C. The virus pellet was then resuspended in amino acid free DMEM (Genaxxon) overnight, 4 °C, with mild shaking. The virus was aliquoted into cryopreservation vials and frozen at -80 °C. The stock was titered as described above. The typical obtained titer was 5 x 10^9 pfu/ml.

Cross-linking of TBEV with SK-N-SH cells

SK-N-SH cells were grown in a 6 well plate to 90 % confluence, washed twice with PBS, and the medium changed to amino acid free DMEM (Genaxxon) supplemented with 100 µg/ml of penicillin-streptomycin mix (PenStrep) (Sigma). The cells were incubated overnight at 37 °C, under a 5 % CO_2 atmosphere. The cells were infected with TBEV at a MOI of 375 for 60 min, with rocking, on ice. Heavy/light disuccinimidyl

454 suberate cross-linker (DSS-H12/D12, Creative Molecules Inc., www. creativemolecules.com) resuspended in
455 dimethylformamide (DMF) was added to final concentrations of 0, 100, 250, 500 and 1000 µM and
456 incubated for 60 min, with rocking on ice. The cross-linking reaction was quenched with a final
457 concentration of 50 mM ammonium bicarbonate with rocking, on ice. The SK-N-SH cell surface proteins
458 with attached TBEV virions were digested off with 1.25 µg trypsin (Promega) and the supernatant collected.
459 Finally, cell debris was removed via centrifugation (16,000 x g, 5 min), the supernatant recovered, and the
460 samples prepared for mass spectrometry (Fig 2).

461 Immunoblot analysis

462 Proteins were resolved in 4-20 % SDS-PAGE, transferred onto a nitrocellulose membrane, and probed using
463 anti-Langat E protein (BEI NR-40318; 1:1000 dilution) and C protein (57) (1:1000 dilution) antibodies in 5 %
464 milk, tris-buffered saline 0.1 % tween-20 (TBST) [70]. The protein bands were visualised using IR800 and
465 IR680-conjugated secondary anti-rabbit (Li-COR, 926-68071) and anti-mouse antibodies (KPL, 072071806)
466 diluted 1:10,000 in tris-buffered saline 0.1 % tween-20 (TBST). The membrane was imaged using the
467 Odyssey infrared imaging system (Li-COR).

468 Preparation of cross-linked samples for mass spectrometry

469 Samples from cross-linking were first denatured with 8 M urea-100 mM ammonium bicarbonate. The
470 cysteine bonds were then reduced with 5 mM tris(2-carboxyethyl) phosphine (37 °C, 60 min, 400 rpm) and
471 alkylated with 10 mM 2-iodoacetamide (22 °C, 30 min, in the dark). Protein digestion was then performed
472 with 0.1 µg/µl sequencing-grade lysyl endopeptidase (Wako chemicals) (37 °C, 2h, 400 rpm). Following the
473 dilution of the sample with 100 mM ammonium bicarbonate to a final urea concentration of 800 mM the
474 proteins were digested further with 0.2 µg/µl trypsin (Promega) (37 °C, 18h, 400 rpm). Digested samples
475 were then acidified with 10% formic acid to a pH of 3.0, and the peptides were subsequently purified with
476 C18 reverse-phase spin columns according to the manufactures protocol (Microspin Column, SS18V, The
477 Nest Group, Inc). Peptides were then dried in a speedvac and reconstituted in 2% acetonitrile, 0.2% formic
478 acid prior to mass spectrometric analyses

Liquid chromatography tandem mass spectrometry

All peptide analyses were performed on a Q Exactive HFX mass spectrometer (Thermo Scientific) connected to an EASY-nLC 1200 ultra-high-performance liquid chromatography system (Thermo Scientific). The peptides were loaded onto an Acclaim PepMap 100 (ID 75µm x 2 cm, 3 µm, 100 Å) pre-column and separated on an EASY-Spray column (Thermo Scientific; ID 75 µm × 25 cm, column temperature 45 °C) operated at a constant pressure of 800 bar. A linear gradient from 4% to 45% of 0.1% formic acid in 80% acetonitrile was run for 50 min at a flow rate of 300 nl/min One full MS scan (resolution 60,000@200 m/z; mass range 350 to 1600 m/z) was followed by MS/MS scans (resolution 15,000@200 m/z) of the 15 most abundant ion signals. The precursor ions were isolated with 2 m/z isolation width and fragmented using higher-energy collisional-induced dissociation at a normalized collision energy of 30. Charge state screening was enabled, and precursors with an unknown charge state and singly charged ions were excluded. The dynamic exclusion window was set to 15 s and limited to 300 entries. The automatic gain control was set to 3×10^6 for MS and 1×10^5 for MS/MS with ion accumulation times of 110 and 60 ms, respectively. The intensity threshold for precursor ion selection was set to 1.7×10^4.

MS data analysis

Raw DDA data was converted to gzipped and Numpressed mzML [71] using MSconvert from the ProteoWizard, v3.0.5930 suite [72]. All data was managed and analysed using openBIS [73]. The acquired spectra were analysed using the search engine X! Tandem (2013.06.15.1-LabKey, Insilicos, ISB) [74], OMSSA (version 2.1.8) [75] and COMET (version 2014.02 rev.2) [76] against an in-house compiled database containing the reviewed *Homo sapiens* reference proteome (UniProt proteome ID UP000005640) and the TBEV proteome (GenBank accession: AWC08512.1), yielding a total of 78121 protein entries and an equal amount of reverse decoy sequences. Full tryptic digestion was used allowing two missed cleavages. Carbamidomethylation (C) was set to static and oxidation (M) to variable modifications, respectively. Mass tolerance for precursor ions was set to 0.2 Da, and for fragment ions to 0.02 Da. Identified peptides were processed and analysed through the Trans-Proteomic Pipeline (TPP v4.7 POLAR VORTEX rev 0, Build

201403121010) using PeptideProphet [77]. The false discovery rate (FDR) was estimated with Mayu (v1.7)[78] and peptide spectrum matches (PSMs) were filtered with protein FDR set to 1% resulting in a peptide FDR >1%. Proteins were filtered to remove hits identified by only 1 unique peptide, and an average spectral count of < 2 across all samples. The protein names and corresponding UniProt ID are given in Supplementary information 1.

Cross-link identification

In total 874 proteins that were identified by 2 or more unique peptides, and an average spectral count of ≥2 across all samples in the DDA data were probed for cross-links. Cross-links between the TBEV structural proteins and host proteins were identified using the pLink2 software package [28]. In order to reduce the search space for cross-link identification the data was analysed in 35 batches. The raw data dependent acquisition data, and compiled FASTA file databases containing a total of 28 protein sequences, from 25 different host proteins and the 3 viral structural protein were used as the software input. Host protein sequences were obtained from UniProt. The TBEV polyprotein sequence was obtained from GenBank (accession: AWC08512.1), the C protein corresponds to residues 1-96, the M protein 206-280 and the E protein 281-776. The following search parameters were used in the pLink2 software: Conventional cross-linking (Higher-energy C-trap dissociation (HCD)), precursor mass tolerance of 20 ppm; fragment mass tolerance of 20 ppm; peptide length of 6-60; peptide mass of 350-6000 Da, up to 3 missed cleavage sites; carbamidomethylation (C) was set to static modification; and oxidation (M) to variable modification. The results were then filtered using a filtering tolerance of ±10 ppm and a separate FDR >5% at the peptide spectrum matches level. 7716 cross-linked spectral observations were observed across all samples, 302 of these were observed in the negative control samples. In total, 247 cross-linked spectral observations in the 0.1-1mM DSS samples corresponded to cross-linked interfaces also identified in negative control samples and were excluded from further analysis.

Homology modelling, structure visualization and measuring cross-link distances

Homology models for the TBEV C protein, immature conformation of the E protein and the prM protein were generated using the I-TASSER (Iterative Threading ASSEmbly Refinement) server [34–36]. A C-score (confidence score for estimating the quality of predicted models by I-TASSER) is generated for each model and can range from -5 to 2, with a higher value signifies a higher confidence and where a C-score > -1.5 is considered good [34–36]. The C-protein homology model was generated using PDB accession 5OW2, and the immature conformation of the E protein, and the prM protein using PDB accession 7L30 as the template. The TBEV polyprotein sequence was obtained from GenBank (accession: AWC08512.1). The sequence for the C protein was obtained from residues 1-96, the E protein residue 281-776, and the prM residues 113-280 in the polyprotein. Generation of the assembled immature virus homology model, and the C-protein dimer was performed in UCSF Chimera [79]. The homology model for the immature virus was generated by superimposing the models for the immature E protein and prM protein onto the assembled immature Spondweni virus (PDB accession 6ZQW) structure, using the MatchMaker function. The homology model for the C protein dimer was generated by superimposing two models of the C protein onto the Zika C protein dimer (PDB accession 5YGH), using MatchMaker. The atomic models were used to position both intraprotein and interprotein cross-links by choosing the distance between Cα atoms in Chimera [24,25].

Networking and clustering analysis

String data were obtained from string database [40] and imported into Cytoscape 3.4 [80] .The following interaction sources were considered: experiments, databases, co-expression, co-occurrence and gene fusion, and interactions with a minimum interaction score of 0.7 are shown. Clusters were generated using the Markov clustering algorithm and gene ontology annotations for each cluster were obtained using GOnet [81].

Data Availability Statement

The datasets generated during and/or analysed in the current study are available in the repositories with the persistent web links: ftp://massive.ucsd.edu/MSV000088272/ [75].

The mass spectrometry data has been deposited to the ProteomeXchange consortium via the MassIVE partner repository https://massive.ucsd.edu/ with the dataset identifier PXD029384 [75].

Acknowledgments

We thank Markku Varjosalo and Johan Malmström for helpful discussions. The work was carried out in the Instruct Centre Finland supported by grants to SJB from the Swedish Research Council reference number 2018-05851; the Academy of Finland grant number 336471, the Sigrid Juselius Foundation and this project (ViBRANT) has also received funding from the European Union's Horizon 2020 Research and Innovation Programme under the Marie Skłodowska-Curie grant agreement number 765042. SVB is a fellow of the Doctoral Programme in Integrative Life Science, University of Helsinki. LIAP is a fellow in the Doctoral Programme in Microbiology and Biotechnology, University of Helsinki. Support from the Swedish National Infrastructure for Biological Mass Spectrometry is gratefully acknowledged.

References

1. Kumar N, Sharma S, Kumar R, Tripathi BN, Barua S, Ly H, et al. Host-Directed Antiviral Therapy. Clin Microbiol Rev. 2020 May 13;33(3):e00168-19, /cmr/33/3/CMR.00168-19.atom.

2. Anasir MI, Zarif F, Poh CL. Antivirals blocking entry of enteroviruses and therapeutic potential. J Biomed Sci. 2021 Dec;28(1):10.

3. Plavec Z, Pöhner I, Poso A, Butcher SJ. Virus structure and structure-based antivirals. Curr Opin Virol. 2021 Dec;51:16–24.

4. Tahir ul Qamar M, Shokat Z, Muneer I, Ashfaq UA, Javed H, Anwar F, et al. Multiepitope-Based Subunit Vaccine Design and Evaluation against Respiratory Syncytial Virus Using Reverse Vaccinology Approach. Vaccines. 2020 Jun 8;8(2):288.

5. Wang N, Shang J, Jiang S, Du L. Subunit Vaccines Against Emerging Pathogenic Human Coronaviruses. Front Microbiol. 2020 Feb 28;11:298.

6. Roulin PS, Murer LP, Greber UF. A Single Point Mutation in the Rhinovirus 2B Protein Reduces the Requirement for Phosphatidylinositol 4-Kinase Class III Beta in Viral Replication. Pfeiffer JK, editor. J Virol. 2018 Sep 12;92(23):e01462-18, /jvi/92/23/e01462-18.atom.

7. Barrass SV, Butcher SJ. Advances in high-throughput methods for the identification of virus receptors. Med Microbiol Immunol (Berl). 2020 Jun;209(3):309–23.

8. Mukherjee S, Sengupta N, Chaudhuri A, Akbar I, Singh N, Chakraborty S, et al. PLVAP and GKN3 Are Two Critical Host Cell Receptors Which Facilitate Japanese Encephalitis Virus Entry Into Neurons. Sci Rep. 2018 Dec;8(1):11784.

9. Shapira SD, Gat-Viks I, Shum BOV, Dricot A, de Grace MM, Wu L, et al. A Physical and Regulatory Map of Host-Influenza Interactions Reveals Pathways in H1N1 Infection. Cell. 2009 Dec;139(7):1255–67.

10. Jäger S, Cimermancic P, Gulbahce N, Johnson JR, McGovern KE, Clarke SC, et al. Global landscape of HIV–human protein complexes. Nature. 2012 Jan 19;481(7381):365–70.

11. Martinez-Martin N, Marcandalli J, Huang CS, Arthur CP, Perotti M, Foglierini M, et al. An Unbiased Screen for Human Cytomegalovirus Identifies Neuropilin-2 as a Central Viral Receptor. Cell. 2018 Aug;174(5):1158-1171.e19.

12. Gordon DE, Jang GM, Bouhaddou M, Xu J, Obernier K, White KM, et al. A SARS-CoV-2 protein interaction map reveals targets for drug repurposing. Nature. 2020 Jul 16;583(7816):459–68.

13. Frei AP, Jeon O-Y, Kilcher S, Moest H, Henning LM, Jost C, et al. Direct identification of ligand-receptor interactions on living cells and tissues. Nat Biotechnol. 2012 Oct;30(10):997–1001.

14. Sobotzki N, Schafroth MA, Rudnicka A, Koetemann A, Marty F, Goetze S, et al. HATRIC-based identification of receptors for orphan ligands. Nat Commun. 2018 Dec;9(1):1519.

15. Srivastava M, Zhang Y, Chen J, Sirohi D, Miller A, Zhang Y, et al. Chemical proteomics tracks virus entry and uncovers NCAM1 as Zika virus receptor. Nat Commun. 2020 Dec;11(1):3896.

16. Terracciano R, Preianò M, Fregola A, Pelaia C, Montalcini T, Savino R. Mapping the SARS-CoV-2–Host Protein–Protein Interactome by Affinity Purification Mass Spectrometry and Proximity-Dependent Biotin Labeling: A Rational and Straightforward Route to Discover Host-Directed Anti-SARS-CoV-2 Therapeutics. Int J Mol Sci. 2021 Jan 7;22(2):532.

17. Coyaud E, Ranadheera C, Cheng D, Gonçalves J, Dyakov BJA, Laurent EMN, et al. Global Interactomics Uncovers Extensive Organellar Targeting by Zika Virus. Mol Cell Proteomics. 2018 Nov;17(11):2242–55.

18. Hauri S, Khakzad H, Happonen L, Teleman J, Malmström J, Malmström L. Rapid determination of quaternary protein structures in complex biological samples. Nat Commun. 2019 Dec;10(1):192.

19. Chowdhury S, Khakzad H, Bergdahl GE, Lood R, Ekstrom S, Linke D, et al. Streptococcus pyogenes Forms Serotype- and Local Environment-Dependent Interspecies Protein Complexes. mSystems. 2021 Oct 26;6(5):e0027121.

20. Kupča AM, Essbauer S, Zoeller G, de Mendonça PG, Brey R, Rinder M, et al. Isolation and molecular characterization of a tick-borne encephalitis virus strain from a new tick-borne encephalitis focus with severe cases in Bavaria, Germany. Ticks Tick-Borne Dis. 2010 Mar;1(1):44–51.

615 21. Han X, Juceviciene A, Uzcategui NY, Brummer-Korvenkontio H, Zygutiene M, Jääskeläinen A, et al.
616 Molecular epidemiology of tick-borne encephalitis virus inIxodes ricinus ticks in Lithuania. J Med Virol. 2005
617 Oct;77(2):249–56.

618 22. Bogovic P. Tick-borne encephalitis: A review of epidemiology, clinical characteristics, and
619 management. World J Clin Cases. 2015;3(5):430.

620 23. Taba P, Schmutzhard E, Forsberg P, Lutsar I, Ljøstad U, Mygland Å, et al. EAN consensus review on
621 prevention, diagnosis and management of tick-borne encephalitis. Eur J Neurol. 2017 Oct;24(10):1214-e61.

622 24. Füzik T, Formanová P, Růžek D, Yoshii K, Niedrig M, Plevka P. Structure of tick-borne encephalitis
623 virus and its neutralization by a monoclonal antibody. Nat Commun. 2018 Dec;9(1):436.

624 25. Rey FA, Heinz FX, Mandl C, Kunz C, Harrison SC. The envelope glycoprotein from tick-borne
625 encephalitis virus at 2 Å resolution. Nature. 1995 May;375(6529):291–8.

626 26. Mandl CW, Allison SL, Holzmann H, Meixner T, Heinz FX. Attenuation of Tick-Borne Encephalitis
627 Virus by Structure-Based Site-Specific Mutagenesis of a Putative Flavivirus Receptor Binding Site. J Virol.
628 2000 Oct 15;74(20):9601–9.

629 27. Renner M, Dejnirattisai W, Carrique L, Martin IS, Karia D, Ilca SL, et al. Flavivirus maturation leads to
630 the formation of an occupied lipid pocket in the surface glycoproteins. Nat Commun. 2021 Dec;12(1):1238.

631 28. Chen Z-L, Meng J-M, Cao Y, Yin J-L, Fang R-Q, Fan S-B, et al. A high-speed search engine pLink 2 with
632 systematic evaluation for proteome-scale identification of cross-linked peptides. Nat Commun. 2019
633 Dec;10(1):3404.

634 29. Ma L, Jones CT, Groesch TD, Kuhn RJ, Post CB. Solution structure of dengue virus capsid protein
635 reveals another fold. Proc Natl Acad Sci. 2004 Mar 9;101(10):3414–9.

636 30. Dokland T, Walsh M, Mackenzie JM, Khromykh AA, Ee K-H, Wang S. West Nile Virus Core Protein.
637 Structure. 2004 Jul;12(7):1157–63.

638 31. Shang Z, Song H, Shi Y, Qi J, Gao GF. Crystal Structure of the Capsid Protein from Zika Virus. J Mol
639 Biol. 2018 Mar;430(7):948–62.

640 32. Zybailov BL. Large Scale Chemical Cross-linking Mass Spectrometry Perspectives. J Proteomics
641 Bioinform [Internet]. 2013 [cited 2021 Jun 10];01(S2). Available from: https://www.omicsonline.org/large-
642 scale-chemical-cross-linking-mass-spectrometry-perspectives-jpb.S2-001.php?aid=12235

643 33. Rinner O, Seebacher J, Walzthoeni T, Mueller LN, Beck M, Schmidt A, et al. Identification of cross-
644 linked peptides from large sequence databases. Nat Methods. 2008 Apr;5(4):315–8.

645 34. Roy A, Kucukural A, Zhang Y. I-TASSER: a unified platform for automated protein structure and
646 function prediction. Nat Protoc. 2010 Apr;5(4):725–38.

647 35. Yang J, Yan R, Roy A, Xu D, Poisson J, Zhang Y. The I-TASSER Suite: protein structure and function
648 prediction. Nat Methods. 2015 Jan;12(1):7–8.

649 36. Yang J, Zhang Y. I-TASSER server: new development for protein structure and function predictions.
650 Nucleic Acids Res. 2015 Jul 1;43(W1):W174–81.

651 37. Merkley ED, Rysavy S, Kahraman A, Hafen RP, Daggett V, Adkins JN. Distance restraints from
652 crosslinking mass spectrometry: Mining a molecular dynamics simulation database to evaluate lysine-lysine
653 distances: Evaluating Lysine-Lysine Distances by MD for XL-MS. Protein Sci. 2014 Jun;23(6):747–59.

654 38. Yang B, Wu Y-J, Zhu M, Fan S-B, Lin J, Zhang K, et al. Identification of cross-linked peptides from
655 complex samples. Nat Methods. 2012 Sep;9(9):904–6.

656 39. Debelyy MO, Waridel P, Quadroni M, Schneiter R, Conzelmann A. Chemical crosslinking and mass
657 spectrometry to elucidate the topology of integral membrane proteins. Gasset M, editor. PLOS ONE. 2017
658 Oct 26;12(10):e0186840.

659 40. Szklarczyk D, Gable AL, Lyon D, Junge A, Wyder S, Huerta-Cepas J, et al. STRING v11: protein–
660 protein association networks with increased coverage, supporting functional discovery in genome-wide
661 experimental datasets. Nucleic Acids Res. 2019 Jan 8;47(D1):D607–13.

662 41. Yuan S, Liu Z, Xu Z, Liu J, Zhang J. High mobility group box 1 (HMGB1): a pivotal regulator of
663 hematopoietic malignancies. J Hematol OncolJ Hematol Oncol. 2020 Dec;13(1):91.

664 42. Pokidysheva E, Zhang Y, Battisti AJ, Bator-Kelly CM, Chipman PR, Xiao C, et al. Cryo-EM
665 Reconstruction of Dengue Virus in Complex with the Carbohydrate Recognition Domain of DC-SIGN. Cell.
666 2006 Feb;124(3):485–93.

667 43. Jones AX, Cao Y, Tang Y-L, Wang J-H, Ding Y-H, Tan H, et al. Improving mass spectrometry analysis
668 of protein structures with arginine-selective chemical cross-linkers. Nat Commun. 2019 Dec;10(1):3911.

669 44. Leitner A, Joachimiak LA, Unverdorben P, Walzthoeni T, Frydman J, Förster F, et al. Chemical cross-
670 linking/mass spectrometry targeting acidic residues in proteins and protein complexes. Proc Natl Acad Sci.
671 2014 Jul 1;111(26):9455–60.

672 45. Malygin AA, Bondarenko EI, Ivanisenko VA, Protopopova EV, Karpova GG, Loktev VB. C-terminal
673 fragment of human laminin-binding protein contains a receptor domain for Venezuelan equine encephalitis
674 and tick-borne encephalitis viruses. Biochem Mosc. 2009 Dec;74(12):1328–36.

675 46. Protopopova EV, Sorokin AV, Konovalova SN, Kachko AV, Netesov SV, Loktev VB. Human laminin
676 binding protein as a cell receptor for the tick-borne encephalitis virus. Zentralblatt Für Bakteriol. 1999
677 Dec;289(5–7):632–8.

678 47. Maginnis MS, Forrest JC, Kopecky-Bromberg SA, Dickeson SK, Santoro SA, Zutter MM, et al. β1
679 Integrin Mediates Internalization of Mammalian Reovirus. J Virol. 2006 Mar 15;80(6):2760–70.

680 48. Feire AL, Roy RM, Manley K, Compton T. The Glycoprotein B Disintegrin-Like Domain Binds Beta 1
681 Integrin To Mediate Cytomegalovirus Entry. J Virol. 2010 Oct;84(19):10026–37.

682 49. Xiao J, Palefsky JM, Herrera R, Berline J, Tugizov SM. The Epstein–Barr virus BMRF-2 protein
683 facilitates virus attachment to oral epithelial cells. Virology. 2008 Jan;370(2):430–42.

684 50. Weigel-Kelley KA, Yoder MC, Srivastava A. α5β1 integrin as a cellular coreceptor for human
685 parvovirus B19: requirement of functional activation of β1 integrin for viral entry. Blood. 2003 Dec
686 1;102(12):3927–33.

687 51. Liu X, Li F, Zhang J, Wang L, Wang J, Wen Z, et al. The ATPase ATP6V1A facilitates rabies virus
688 replication by promoting virion uncoating and interacting with the viral matrix protein. J Biol Chem. 2021
689 Jan;296:100096.

690 52. Liu Y-G, Chen Y, Wang X, Zhao P, Zhu Y, Qi Z. Ezrin is essential for the entry of Japanese encephalitis
691 virus into the human brain microvascular endothelial cells. Emerg Microbes Infect. 2020 Jan 1;9(1):1330–
692 41.

693 53. Liu Q, Huang X, Zhao D, Han K, Liu Y, Yang J, et al. Identification of heat shock protein A9 as a
694 Tembusu virus binding protein on DF-1 cells. Virus Res. 2017 Jan;227:110–4.

695 54. Jindadamrongwech S, Thepparit C, Smith DR. Identification of GRP 78 (BiP) as a liver cell expressed
696 receptor element for dengue virus serotype 2. Arch Virol. 2004 May;149(5):915–27.

697 55. Khongwichit S, Sornjai W, Jitobaom K, Greenwood M, Greenwood MP, Hitakarun A, et al. A
698 functional interaction between GRP78 and Zika virus E protein. Sci Rep. 2021 Jan 11;11(1):393.

699 56. Nain M, Mukherjee S, Karmakar SP, Paton AW, Paton JC, Abdin MZ, et al. GRP78 Is an Important
700 Host Factor for Japanese Encephalitis Virus Entry and Replication in Mammalian Cells. J Virol. 2017 Mar
701 15;91(6):e02274-16.

702 57. Zhao D, Liu Q, Han K, Wang H, Yang J, Bi K, et al. Identification of Glucose-Regulated Protein 78
703 (GRP78) as a Receptor in BHK-21 Cells for Duck Tembusu Virus Infection. Front Microbiol. 2018 Apr 9;9:694.

704 58. Dana RC, Welch WJ, Deftos LJ. Heat shock proteins bind calcitonin. Endocrinology. 1990
705 Jan;126(1):672–4.

706 59. Oka OBV, Pringle MA, Schopp IM, Braakman I, Bulleid NJ. ERdj5 is the ER reductase that catalyzes
707 the removal of non-native disulfides and correct folding of the LDL receptor. Mol Cell. 2013 Jun
708 27;50(6):793–804.

709 60. Evensen NA, Kuscu C, Nguyen H-L, Zarrabi K, Dufour A, Kadam P, et al. Unraveling the role of
710 KIAA1199, a novel endoplasmic reticulum protein, in cancer cell migration. J Natl Cancer Inst. 2013 Sep
711 18;105(18):1402–16.

712 61. Cuevas EP, Eraso P, Mazón MJ, Santos V, Moreno-Bueno G, Cano A, et al. LOXL2 drives epithelial-
713 mesenchymal transition via activation of IRE1-XBP1 signalling pathway. Sci Rep. 2017 Mar 23;7:44988.

714 62. Bellani S, Mescola A, Ronzitti G, Tsushima H, Tilve S, Canale C, et al. GRP78 clustering at the cell
715 surface of neurons transduces the action of exogenous alpha-synuclein. Cell Death Differ. 2014
716 Dec;21(12):1971–83.

717 63. Bhattacharjee G, Ahamed J, Pedersen B, El-Sheikh A, Mackman N, Ruf W, et al. Regulation of tissue
718 factor--mediated initiation of the coagulation cascade by cell surface grp78. Arterioscler Thromb Vasc Biol.
719 2005 Aug;25(8):1737–43.

720 64. Philippova M, Ivanov D, Joshi MB, Kyriakakis E, Rupp K, Afonyushkin T, et al. Identification of
721 Proteins Associating with Glycosylphosphatidylinositol- Anchored T-Cadherin on the Surface of Vascular
722 Endothelial Cells: Role for Grp78/BiP in T-Cadherin-Dependent Cell Survival. Mol Cell Biol. 2008 Jun
723 15;28(12):4004–17.

724 65. Honda T, Horie M, Daito T, Ikuta K, Tomonaga K. Molecular Chaperone BiP Interacts with Borna
725 Disease Virus Glycoprotein at the Cell Surface. J Virol. 2009 Dec;83(23):12622–5.

726 66. Mayer MP, Gierasch LM. Recent advances in the structural and mechanistic aspects of Hsp70
727 molecular chaperones. J Biol Chem. 2019 Feb;294(6):2085–97.

728 67. Elfiky AA, Ibrahim IM. Zika virus envelope – heat shock protein A5 (GRP78) binding site prediction. J
729 Biomol Struct Dyn. 2021 Sep 22;39(14):5248–60.

730 68. van der Schaar HM, Rust MJ, Chen C, van der Ende-Metselaar H, Wilschut J, Zhuang X, et al.
731 Dissecting the Cell Entry Pathway of Dengue Virus by Single-Particle Tracking in Living Cells. Farzan M,
732 editor. PLoS Pathog. 2008 Dec 19;4(12):e1000244.

733 69. Suksanpaisan L, Susantad T, Smith DR. Characterization of dengue virus entry into HepG2 cells. J
734 Biomed Sci. 2009;16(1):17.

735 70. Iacono-Connors LC, Smith JF, Ksiazek TG, Kelley CL, Schmaljohn CS. Characterization of Langat virus
736 antigenic determinants defined by monoclonal antibodies to E, NS1 and preM and identification of a
737 protective, non-neutralizing preM-specific monoclonal antibody. Virus Res. 1996 Aug;43(2):125–36.

738 71. Teleman J, Dowsey AW, Gonzalez-Galarza FF, Perkins S, Pratt B, Röst HL, et al. Numerical
739 Compression Schemes for Proteomics Mass Spectrometry Data. Mol Cell Proteomics. 2014 Jun;13(6):1537–
740 42.

741 72. Chambers MC, Maclean B, Burke R, Amodei D, Ruderman DL, Neumann S, et al. A cross-platform
742 toolkit for mass spectrometry and proteomics. Nat Biotechnol. 2012 Oct;30(10):918–20.

743 73. Bauch A, Adamczyk I, Buczek P, Elmer F-J, Enimanev K, Glyzewski P, et al. openBIS: a flexible
744 framework for managing and analyzing complex data in biology research. BMC Bioinformatics.
745 2011;12(1):468.

746 74. Craig R, Beavis RC. A method for reducing the time required to match protein sequences with
747 tandem mass spectra. Rapid Commun Mass Spectrom. 2003 Oct 30;17(20):2310–6.

748 75. Geer LY, Markey SP, Kowalak JA, Wagner L, Xu M, Maynard DM, et al. Open Mass Spectrometry
749 Search Algorithm. J Proteome Res. 2004 Oct;3(5):958–64.

750 76. Eng JK, Jahan TA, Hoopmann MR. Comet: An open-source MS/MS sequence database search tool.
751 PROTEOMICS. 2013 Jan;13(1):22–4.

752 77. Keller A, Nesvizhskii AI, Kolker E, Aebersold R. Empirical Statistical Model To Estimate the Accuracy
753 of Peptide Identifications Made by MS/MS and Database Search. Anal Chem. 2002 Oct 1;74(20):5383–92.

754 78. Reiter L, Claassen M, Schrimpf SP, Jovanovic M, Schmidt A, Buhmann JM, et al. Protein
755 Identification False Discovery Rates for Very Large Proteomics Data Sets Generated by Tandem Mass
756 Spectrometry. Mol Cell Proteomics. 2009 Nov;8(11):2405–17.

757 79. Pettersen EF, Goddard TD, Huang CC, Couch GS, Greenblatt DM, Meng EC, et al. UCSF Chimera?A
758 visualization system for exploratory research and analysis. J Comput Chem. 2004 Oct;25(13):1605–12.

759 80. Shannon P. Cytoscape: A Software Environment for Integrated Models of Biomolecular Interaction
760 Networks. Genome Res. 2003 Nov 1;13(11):2498–504.

761 81. Pomaznoy M, Ha B, Peters B. GOnet: a tool for interactive Gene Ontology analysis. BMC
762 Bioinformatics. 2018 Dec;19(1):470.

763 Supporting information captions

764 **S1 Table: DDA analysis of viral and host protein in all samples** (XLSX).

765 **S2 Table: Cross-linking dataset** Identified cross-linked peptides, corresponding proteins, E-values and SVM

766 scores for each cross-linked spectral observation (XLSX).

S3 Table: Filtered cross-linking dataset Cross-linking dataset (S2 Table) filtered to remove spectral observations corresponding to unique cross-links identified by less than 2 spectral observations with SVM scores < 0.355 (XLSX).

S4 Table: GO analysis of host proteins GO analysis of the 59 host proteins shown to interact with the surface of TBEV in the filtered cross-linking dataset (S3 Table) (XLSX).

S1 File: Correlation between number of cross-linked spectral observations, protein abundance and protein lysine content Table showing the number of cross-linked spectral observations, the average protein abundance calculated in the DDA analysis (S1 Table) and the number of lysines for 101 randomly selected proteins. Scatter graphs show no correlation between the number of cross-linked spectral observations and the number of lysines for the proteins, and no correlation between the number of cross-linked spectral observations and the protein abundance (XLSX).

S1 Fig: Box and whisker plot of the E-value for the intraviral cross-links, plotted against the distance between the cross-linked residues for each cross-link. The smallest distance out of the mature and immature calculated distances, and the C protein dimer or monomer distances is plotted. The mean E-value is marked with a cross.